

Evolution of Galaxy Clustering

J.S.Bagla

*Institute of Astronomy, University of Cambridge, Madingley Road, Cambridge CB3 0HA, U.K.
E-mail: jasjeet@ast.cam.ac.uk*

2 December 2024

ABSTRACT

We study the evolution of correlation function of dark matter halos in the CDM class of models. We show that the halo correlation function does not evolve in proportion with the correlation function of the underlying mass distribution. Earliest halos to collapse, which correspond to rare peaks in the density field, cluster very strongly. The amplitude of halo correlation function *decreases* from its initial, large, value. This decrease continues till the average peaks have collapsed, after which, the amplitude grows at a slow rate. This behaviour is shown to be generic and the epoch of minimum amplitude depends only on the *rms* fluctuations in mass at the relevant scale and, to a much smaller extent, on the slope of the power spectrum at that scale. We discuss the relevance of this result for interpretation of observations of galaxy clustering.

Key words: Galaxies : Formation – Cosmology : Theory – Early Universe, Large Scale Structure of the Universe

1 INTRODUCTION

It is believed that structures like galaxies and clusters of galaxies formed by gravitational amplification of small perturbations. This implies that clustering in the mass distribution in the Universe always increases with time. In this model, galaxies form in highly over-dense halos of dark matter. Evolution of galaxy clustering and its relation to the clustering in the underlying mass distribution is an important question that needs to be addressed before we can correctly interpret the observations of galaxy clustering. In this paper we discuss one approach to this problem and comment on the relevance of our results for interpretation of observations of galaxy clustering and its evolution.

Clustering properties of halos have been studied by many authors (See, for example, Gelb and Bertschinger (1994b)). These studies show that there is no simple, scale independent relation between the correlation functions for the mass distribution and halos. Evolution of clustering properties of halos has been studied by Brainerd and Villumsen (1994). They computed the halo-halo correlation function and found that it evolves very slowly in most cases. In some cases they found a *decreasing* phase before the amplitude of the halo correlation function starts growing. Recently, some authors have studied the effects of a decreasing correlation function, and an epoch of minimum amplitude of clustering, on the angular correlation function of galaxies (Ogawa, Roukema and Yamashita 1997).

In this paper we argue that the halo correlation function, for halos above a given mass, has a generic behaviour: its amplitude is very large at early times, and de-

creases very rapidly. The amplitude reaches a minima and then increases at a slow rate.

The paper is organised as follows: §2 outlines a model for evolution of halo clustering. In §3 we describe the numerical simulations used for testing the model. This section also contains details of our approach for identifying halos and calculation of the halo correlation function. Results are presented in §4 and in §5 we discuss the generalisation to galaxy clustering and the relevance of our results for interpretation of observations. We summarise the main conclusions in §6.

2 THE HALO GRAIL

In most models of structure formation, the initial density field is assumed to be a Gaussian random field. Gravitational instability leads to amplification of density perturbations, and over-dense regions collapse to form virialised halos. If the threshold density contrast for formation of halos is much larger than the *rms* dispersion in density contrast, as is the case at early times, only a few rare peaks collapse into halos. These peaks are expected to cluster strongly compared to the almost smooth mass distribution. These peaks are not good tracers of the underlying mass distribution. On the other hand, if the threshold is less than, or comparable to, the *rms* dispersion, almost all peaks collapse to form halos and the halo number density traces the mass distribution at scales (much) larger than the typical halo-halo separation. Thus we expect the halos to become “better” tracers of the mass distribution with time. In the following discussion, we

quantify these statements and present a simple model for evolution of the halo correlation function.

Consider the distribution of halos of mass M , or larger, before typical halos of this mass have collapsed. To quantify this, we first define a *bias* parameter $\nu(M, z) = \delta_c/\sigma(M, z)$, where $\sigma(M)$ is the (linearly extrapolated) *rms* dispersion in the density contrast at mass scale M and δ_c is the linearly extrapolated density contrast at which halos are expected to collapse and virialise. We use the value $\delta_c = 1.68$, obtained from the spherical top hat collapse model (Gunn and Gott 1972). Most halos of mass M collapse when $\nu(M) \approx 1$. At early times, $\nu \gg 1$, and the number density of collapsed halos is very small (compared to, say, $\bar{\rho}/M$, where $\bar{\rho}$ is the background density at that epoch). We can write the linear correlation function of these rare peaks, at scales where $\frac{\xi(M, r)}{\xi(M, 0)} \ll 1$, as (Bardeen et. al. 1986)

$$\xi_H(M, r) = \exp \left[\nu^2 \frac{\xi(M, r)}{\xi(M, 0)} \right] - 1 \quad (1)$$

Here $\xi(M, r)$ is the correlation function of the smoothed density field (smoothed at mass scale M) evaluated at scale r , and ξ_H is the halo correlation function. The halo correlation has an exponentially large amplitude over the range of scales where $\nu^2 \frac{\xi(M, r)}{\xi(M, 0)} > 1$. Even at very large scales, the halo correlation function has a much larger amplitude as compared to the mass correlation ($\xi_H(M, r) \simeq \nu^2 \frac{\xi(M, r)}{\xi(M, 0)}$). It follows that at early times, the halo correlation function has a much larger amplitude than the mass correlation function at all scales.

Time evolution of the linear correlation function for halos, as described in eqn.(1), is controlled by the function ν .

$$\nu(M, z) = \frac{\delta_c}{\sigma(M, z)} = \frac{D_+(z_c)}{D_+(z)} = \frac{1+z}{1+z_c}. \quad (2)$$

Here D_+ is the growing mode for density perturbations in linear theory and z_c is fixed by requiring $\nu(M, z_c) = 1$. The last equality is valid only in the Einstein-deSitter Universe as in that case $D_+(z) = (1+z)^{-1}$. D_+ is a monotonically increasing function of time, implying that ν is a monotonically decreasing function. *Therefore, at early times, the amplitude of correlation function of halos is a rapidly decreasing function of time.*

Eqn.(1) gives only the linearly extrapolated correlation function for halos. However, the qualitative behaviour, being exponentially strong, should survive the non-linear evolution.

At later epochs, when $\nu(M) \approx 1$, eqn.(1) is no longer valid. By this time, most halos of mass M have collapsed and the halo distribution begins to trace the underlying mass distribution. Therefore, further evolution of the halo distribution must reflect the growth of density perturbations. There is another way of explaining this for hierarchical models: low mass halos merge and give rise to more massive halos. As gravity brings halos closer for merger, the halo correlation function must increase. However, the rate of growth of correlation function will be slow as *anti-biased* halos continue to collapse for some time.

Thus, there are two effects that contribute to the evolution of correlation function of halos: The *intrinsic* correlation function of halos that have collapsed, and, gravitational instability. These effects act in opposite directions. At early times the rapidly changing *intrinsic* correlation function of

| Simulation | Physical Scale (h^{-1} Mpc) | Mass ($10^{10} M_\odot$) | Range in Redshift |
|------------|-----------------------------------|-------------------------------|-------------------|
| G.5-0.6-1 | 0.1 | 0.056 | 10 – 2 |
| G.5-0.6-2 | 0.2 | 0.45 | 6 – 1 |
| G.5-0.6-3 | 0.3 | 1.5 | 5 – 0.5 |
| G.5-0.6-4 | 0.5 | 7.0 | 4 – 0 |
| G.5-0.6-5 | 0.7 | 19.2 | 3 – 0 |
| G.5-0.6-6 | 1.0 | 56 | 2 – 0 |
| G.5-0.6-7 | 1.3 | 123 | 1 – 0 |

Table 1. This table lists the parameters of simulations used in this paper. The first column gives the name of the simulation. The second column gives the physical scale corresponding to one grid cell, in units of h^{-1} Mpc, the simulation box is a cube with 128^3 such cells. The third column gives the mass of one N-Body particle in units of $10^{10} M_\odot$ and the fourth column lists the range of redshifts over which the halo clustering was studied for the given simulation.

the few halos that have collapsed dominates. At late times, gravitational clustering takes over, leading to growth of the correlation function. Therefore, at some intermediate epoch, these effects must cancel each other leading to a stationary amplitude of the halo correlation function. This is likely to happen when $\nu \approx 1$.

3 NUMERICAL SIMULATIONS

We used a set of simulations of the standard CDM model, normalised so that the linearly extrapolated *rms* fluctuations in density, smoothed with a spherical top hat window function at the scale of $8h^{-1}$ Mpc, is $\sigma_8 = 0.6$. All simulations were done with a PM (Particle-Mesh) code and 128^3 particles in a box with the same number of cells. Parameters of simulations used here are described in table 1.

We used the friends-of-friends (FOF) algorithm with a linking length of 0.2 grid length to identify dense halos. For the purpose of computing the correlation function, we used halos with 10 or more particles. This was done to avoid noise due to erroneous detections of smaller groups.

In principle, we should identify halos with mass in a given range and compute the correlation function for these at different epochs. However, the following reasons force us to use a different strategy:

- The FOF algorithm, for $l = 0.2$, is known to link dynamically distinct halos (Gelb and Bertschinger 1994a). (Smaller linking lengths tend to dissolve some halos.) This leads to an incorrect estimate of the mass of halos. We will also underestimate the number of close pairs of halos, and therefore, the amplitude of the correlation function.
- Finite mass resolution in numerical simulations leads to the over-merging problem (Moore, Katz and Lake 1996). The over-merging problem in collisionless simulations makes it difficult to estimate the number of halos of a given mass that may have survived inside bigger halos.

These problems are particularly serious at late times when the number of halos is large and there are many cluster sized halos present in the system. To circumvent these problems we adopt a different approach. We do not consider halos as being one unit each. Instead, we assign a weight, proportional to the mass, to each halo. Operationally, this is equivalent to computing the correlation function of particles

Figure 1. This figure shows the distribution of particles in a slice from the simulation G.5-0.6-1. The thickness of the slice is $3h^{-1}\text{Mpc}$. The halo particles are marked as thick points. To highlight the highly non-uniform distribution of halos, we have drawn a box in the lower left corner of each frame that shows the region that should contain one halo if these were distributed uniformly. The upper panel shows the slice at $z = 8$ and the lower panel shows the same at $z = 6$.

contained in these halos. This strategy is also appropriate for studying the evolution of galaxy correlation function, as galaxies are known to survive inside groups and clusters of galaxies. Although our method ignores the large range in masses of galaxies by using this particular method, we are able to include the contribution of very massive halos that are likely to contain many galaxies.

Figure 1. This figure shows the same slice at $z = 4$ (upper panel) and $z = 2$ (lower panel).

4 RESULTS

To show that halos cluster very strongly at early times, we have plotted the halos, along with a random subset of all the N-Body particles, in a slice from the simulation G.5-0.6-1. We have shown the same slice at four redshifts; $z = 8, 6, 4$ and 2 . The thickness of the slice is $3h^{-1}\text{Mpc}$ (comoving). The particles in halos ($M_{halo} \geq 5.6 \times 10^9 M_{\odot}$) are shown as thick dots and the N-Body particles are shown as thin dots. A box on the bottom-left corner shows the *projected area per halo*, if the halos were distributed uniformly then there should be one halo in a region of this size on an average. It is clear from this figure that the halo distribution is

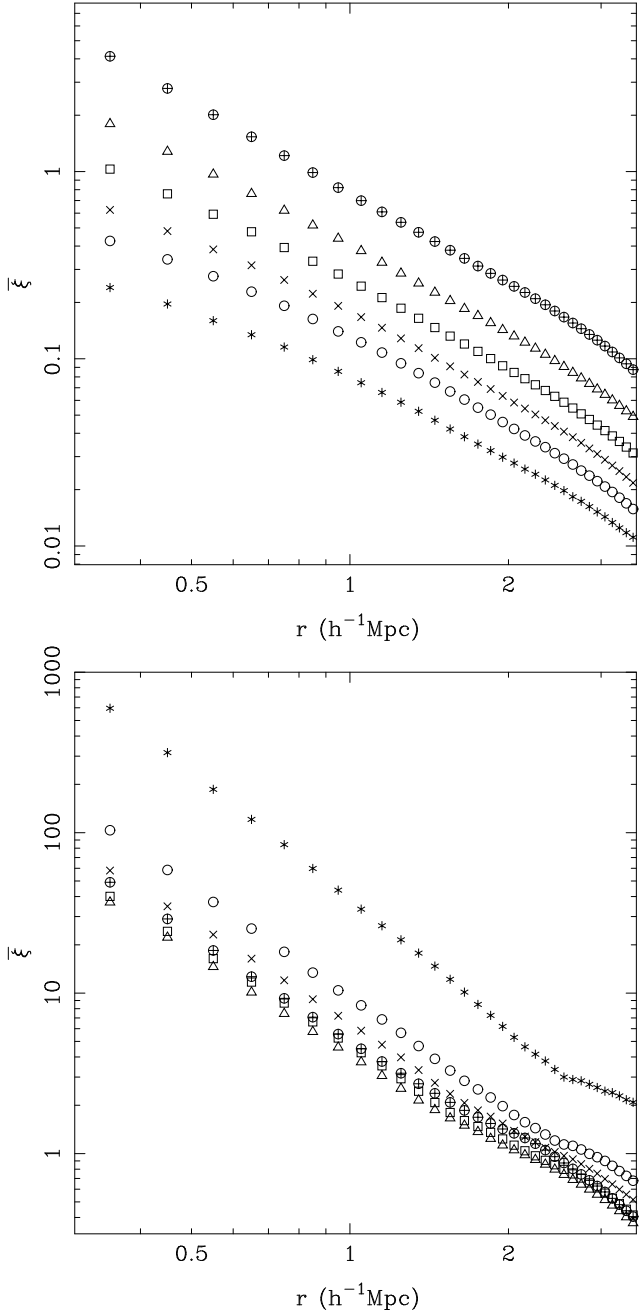


Figure 2. This figure shows the results for simulation G.5-0.6-1. The averaged correlation function $\bar{\xi}$ is shown as a function of scale $r(h^{-1}\text{Mpc})$. The top panel shows the evolution of clustering in the total mass distribution. As redshift decreases, $\bar{\xi}$ increases monotonically. We have shown the points for $z = 8$ (*), $z = 6$ (○), $z = 5$ (×), $z = 4$ (□), $z = 3$ (△) and $z = 2$ (⊕). The amplitude of the halo correlation function decreases rapidly at early times, reaches a minima at $z = 2$ ($\nu = 0.96$) and then increases again.

very non-uniform at early times even though the underlying mass distribution is largely homogeneous. It is also obvious that the halo distribution develops along the ‘‘skeleton’’ of the late time mass distribution. Halos form along filaments and pancakes, or their intersections. Other simulations also show a similar pattern of evolution. (To see the variation

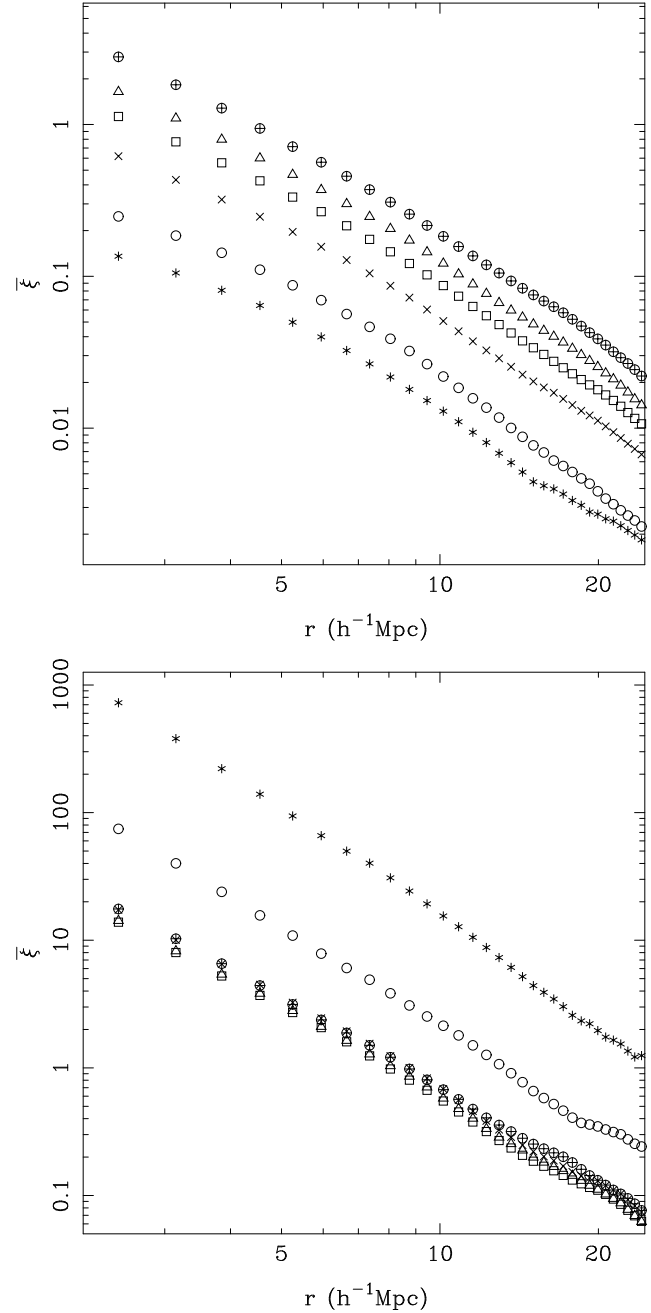


Figure 3. Same as fig.2, this figure compares the evolution of clustering of mass and halos for the simulation G.5-0.6-5. We have shown the points for $z = 3$ (*), $z = 2$ (○), $z = 1$ (×), $z = 0.5$ (□), $z = 0.25$ (△) and $z = 0$ (⊕). In this case the minimum amplitude of the halo correlation function is reached at $z = 0.5$ ($\nu = 1.1$).

with linking length used for locating halos, see the plots in Brainerd and Villumsen (1994).)

We describe the clustering properties using the averaged two point correlation function $\bar{\xi}(r)$

$$\bar{\xi}(r) = \frac{3}{r^3} \int_0^r x^2 \xi(x) dx = \frac{3J_3(r)}{r^3} \quad (3)$$

where $\xi(x)$ is the two point correlation function. The averaged correlation function is a measure of the excess neigh-

neighbours around a typical point in a sphere of radius r , whereas the two point correlation function is a measure of excess neighbours in a spherical shell at r .

We have plotted the averaged correlation function for the mass distribution and the halo distribution in fig.2 (G.5-0.6-1) and fig.3 (G.5-0.6-5). The top panel of each figure shows the correlation function for mass and the lower panel shows the correlation function for mass contained within halos. These figures show that the clustering in mass increases monotonically, as expected. These figures also confirm that the amplitude of the halo correlation function is large at early times and it decreases very rapidly. The amplitude of the halo correlation function reaches a minima at $\nu \approx 1.0$ and then increases again. In the simulations used here, we find that the amplitude of halo correlation function reaches its minimum at lower ν , i.e. at a later epoch than $\nu = 1$, for more negative indices. We find the range $\nu_{min} = 0.96$ (G.5-0.6-1; $n_{eff} = -2.4$) to $\nu_{min} = 1.1$ (G.5-0.6-5; $n_{eff} = -1.9$). Here, the index n_{eff} is defined as

$$n_{eff} = -3 + \frac{\partial \ln \sigma^2(r)}{\partial \ln r} \quad (4)$$

We are studying the variation of ν_{min} with the index for power law models.

These figures also show that the correlation function for low mass halos is smaller than the correlation function of more massive halos at the same epoch. This follows from the monotonic increase in ν with M for fixed z .

The shape of both the mass correlation and halo correlation changes with time. The halo correlation function becomes less steep with time, whereas the mass correlation function becomes steeper. If we compare the shape and amplitude of the halo and mass correlation function at $z = 0$ in fig.3 then it is apparent that the halo correlation function has a higher amplitude and it is steeper than the mass correlation function. To quantify this, we have plotted the $bias^*$ as a function of scale for these halos in fig.4. The correlation bias is defined as

$$b^2(r, z) = \frac{\bar{\xi}_H(r, z)}{\bar{\xi}(r, z)}. \quad (5)$$

The correlation bias is a function of scale and redshift. Fig.4 shows this function ($M_{halo} \geq 2 \times 10^{12} M_\odot$) at the present epoch. Bias increases at scales smaller than about $10 h^{-1} \text{Mpc}$ but is essentially a constant at larger scales. The qualitative behaviour of the correlation bias in G.5-0.6-5 does not evolve very strongly in time. The scale dependence of correlation bias has important implications for inversion of galaxy power spectrum to obtain the initial power spectrum (see §5.1).

Fig.5 (upper panel) shows the variation of correlation bias at two comoving scales ($5 h^{-1} \text{Mpc}$ and $15 h^{-1} \text{Mpc}$) as a function of redshift. At early times the bias varies very rapidly but at late times the variation is almost linear. For comparison, we have plotted (solid lines) the expression for variation of bias suggested by Fry (1996) through the low redshift points.

$$b = \frac{z_* + b_*}{1 + z_*} + z \frac{b_* - 1}{1 + z_*} = 1 + (1 + z)(b_0 - 1). \quad (6)$$

* Note that this bias is different from ν defined earlier. This degeneracy in nomenclature is unfortunate and we will use the term correlation bias for this one to avoid confusion.

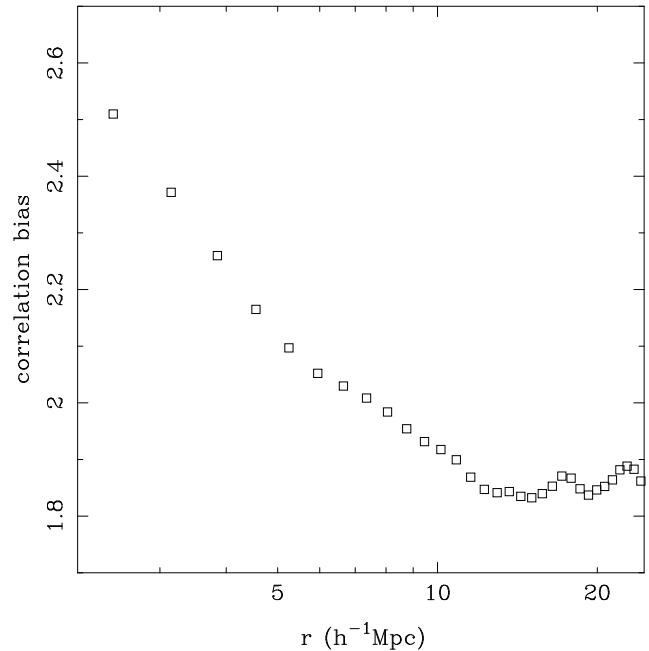


Figure 4. This figure shows the correlation bias at $z = 0$ for halos of mass $M \geq 2 \times 10^{12} M_\odot$ as a function of scale. It is clear that the bias varies with scale at small scales but fluctuates around a constant value at larger scales.

Here, z_* is the epoch at which halos/galaxies form and b_* is the local bias at that epoch and is defined as the ratio of density contrast in galaxies to the density contrast in mass (Fry 1996). In this model, all the halos are assumed to form at the same redshift z_* . b_0 is the bias at $z = 0$. This equation shows that in this model, an unbiased set of tracers always remain unbiased. At early times, the combined assumption of conservation of the numbers of halos and a local bias[†] is not valid as the rate of formation of halos is high and these are not fair tracers of the mass distribution.

This model cannot reproduce the decreasing phase for the amplitude of the correlation function. The combination $b(z)/(1 + z)$ must decrease in forward evolution for the decreasing phase to be reproduced correctly.

Matarrese et al. (1997) have discussed many different ansatz for evolution of correlation bias in the redshift space. In general, they get the following form for correlation bias

$$b(z) = c_1 + c_2(1 + z)^\beta \quad (7)$$

where some of the parameters can be fixed/related by choosing an appropriate ansatz. As is apparent from fig.5, no single power law can fit the bias seen in simulations for the entire range of redshifts. However, for a suitable choice of parameters, this functional form does satisfy the criterion given above for a decreasing correlation function. We have checked that this form matches well with the data points up to $z = 1$ for $\beta \simeq 2$. This range of redshifts includes a

[†] Local bias is defined as the ratio between density contrasts in galaxy number and the underlying mass distribution. The model by Fry (1996) assumes that the local bias is independent of position.

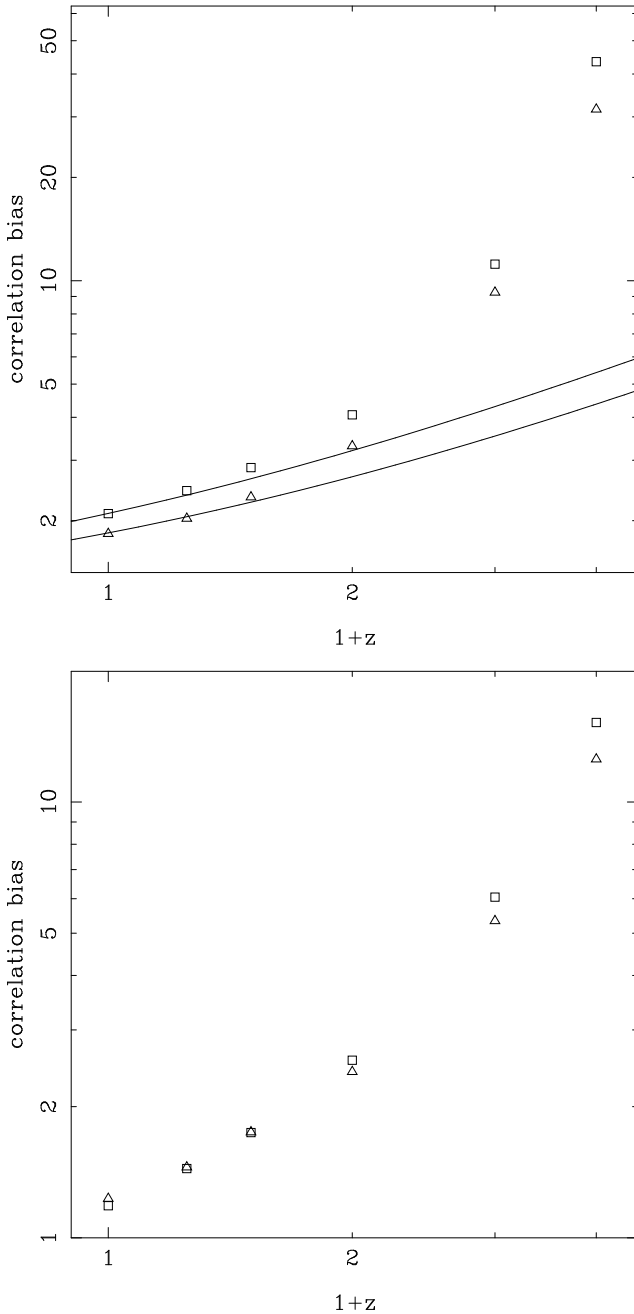


Figure 5. This figure shows correlation bias at a fixed scale (\square : $5h^{-1}\text{Mpc}$ and \triangle : $15h^{-1}\text{Mpc}$) as a function of redshift for the simulation G.5-0.6-5. The upper panel shows bias computed using the mass weighted scheme. At late times, the variation of bias is almost linear in redshift and the expression suggested by Fry (1996) (solid lines through low redshift points) is a reasonable fit to the data. The variation of bias at early times is very rapid and cannot be described by the model as the assumptions of local bias and conservation of halos are not valid. The lower panel shows correlation bias, where the halo correlation function is computed by assuming each halo to be one unit. This panel shows that the relative bias at the two scales crosses unity around $\nu \simeq 1$. This is a reflection of the over-merging and linking of distinct halos. These result in an underestimate of halos at smaller separation and hence lowering of the correlation bias at small scales.

mild decrease in the correlation function between $z = 1$ and $z = 0.5$.

The problems due to linking of distinct halos and over merging, listed in §3, create serious problems at late times. We chose to work with mass weighted correlation function of halos instead of the simple halo-halo correlation in order to avoid this problem. However, at early times, it may be better to compute the unweighted halo correlation function. For comparison, we computed the unweighted halo correlation function. This leads to a lower, and perhaps a more reliable, value for correlation bias at early times. The lower panel of fig.5 shows correlation bias for the same two scales computed with this method. In this case, the linear bias (Fry 1996) fails to reproduce the variation observed in simulations.

Fig.5 also shows that the correlation bias at the two scales shown here evolves slightly differently. This is a manifestation of the changing shape of the halo and mass correlation functions.

The lower panel of fig.5 shows that the relative bias at the two scales crosses unity around $\nu \simeq 1$. This is a reflection of the over-merging and linking of distinct halos. These result in an underestimate of halos at smaller separation and hence lowering of the correlation bias at small scales.

Many authors have constructed analytical models to understand the evolution of bias (Mo and White 1996; Catelan et al. 1997 and references cited therein) field where the concept is generalised from statistical bias (only a function of scale and epoch) to a bias that depends both on position and epoch. In these models (including Fry (1996)) the mapping from the initial halo distribution to the final one is done using perturbative or approximate methods. We have presented comparison with Fry (1996) as it is the simplest of this class of models. In other, more complex models, a comparison with halo correlation function as it is computed here cannot be carried out in a straightforward manner.

5 DISCUSSION

In §4 we described evolution of the correlation function for mass contained in halos of mass greater than a given cutoff. These results, when applied to galaxies, have many important implications. In §5.1, we will discuss the calculation of the initial power spectrum from the observed galaxy correlation function in view of the results presented in §4. In §5.2 we turn to the question of evolution of galaxy/quasar clustering and its relation with the evolution of halo clustering. Lastly, we outline some implications of these results for evolution of the inter-galactic medium and galaxy formation models in §5.3.

5.1 Galaxy Correlation Function and the Initial Power Spectrum

In this section, we assume that the halo distribution and galaxy distribution are the same at the present epoch. This is a reasonable assumption for studying galaxy clustering at a given epoch, as long as the mass of halos is not too different from the mass of typical galaxies studied in surveys.

The shapes of mass and galaxy correlation functions are different, even at late times (fig.2, fig.3 and fig.4). These differences introduce errors in calculation of the initial power

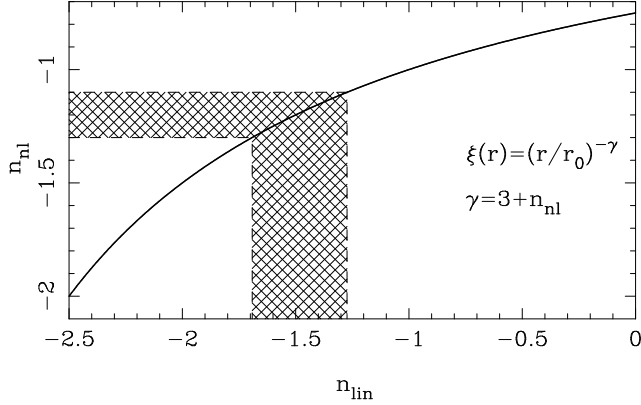


Figure 6. This figure shows the non-linear index of the power spectrum as a function of the linear index in the quasi-linear regime ($1 \leq \bar{\xi} \leq 200$). This relation is derived using a power law fit to the relation between the linear and evolved correlation (Hamilton et al. 1991). We have shown a horizontal shaded region to mark the region $\gamma = 1.8 \pm 0.1$. This translates into a linear index of $\gamma_{lin} \simeq 1.5 \pm 0.2$, marked by the vertical shaded region. This demonstrates the amplification of uncertainty in the index of power spectrum in the inversion process.

spectrum from observations of galaxy clustering using scaling relations (Peacock and Dodds 1996).

Fig.6 shows the non-linear index n_{nl} as a function of the linear index n_{lin} of the averaged correlation function. We define n_{nl} as in eqn.(4) except that σ^2 is replaced by $\bar{\xi}$. This relation between the indices is obtained by using the power law fit (Bagla and Padmanabhan 1997) in the quasi-linear regime ($1 \leq \bar{\xi} \leq 200$)[‡] to the scaling relation between the linear and the non-linear correlation function (Hamilton et al. 1991). This figure shows that this relation flattens out for indices above $n_{nl} = -1$. Two reasons contribute to this flattening:

- The index $n_{lin} = -1$ is a “critical index” in the sense that power spectra with an index close to $n_{lin} = -1$ change shape so that n_{nl} is closer to this critical index in the quasi-linear regime (Bagla and Padmanabhan 1997).
- Gravitational clustering of hierarchical models ($n > -3$) restricts the non-linear indices below $n_{nl} \leq 3/\bar{\xi}$ (Bagla and Padmanabhan 1997). In other words, the non-linear index of the power spectrum must be in the range $-3 \geq n_{nl} \geq 0$, irrespective of the initial index.

Gravitational instability acts to decrease (but not to erase) the differences between different initial conditions. Therefore, any uncertainties in the non-linear mass correlation function translate into much larger uncertainties in the initial power spectrum. The difference in the shape/slope and the amplitude of the galaxy correlation function and the mass correlation function is one such uncertainty.

In order to assess this amplification of uncertainty in a quantitative manner, we have mapped a narrow range of non-linear indices, $n_{nl} = -1.2 \pm 0.1$ ($\gamma = 1.8 \pm 0.1$), to the corresponding linear indices. The permitted range of linear

[‡] For a power law correlation function, $\bar{\xi} = 3\xi/(3 - \gamma)$. Thus for $\gamma = 1.8$, as suggested by observations, this relation between the indices can be used up to about $8h^{-1}\text{Mpc}$.

indices is much larger ($n_{lin} \simeq -1.5 \pm 0.2$; $\gamma \simeq 1.5 \pm 0.2$). Therefore, even a small error in the non-linear index[§] of the power spectrum can lead to a much larger error in the linear power spectrum. In addition to the uncertainty in slope, uncertainty in amplitude also contributes to the error.

The above discussion shows that inverting the galaxy correlation function to determine the initial power spectrum leads to amplification of uncertainties. This is especially true of non-linear scales where correlation bias depends on scale. At larger scales, bias is expected to be scale independent and the main source of error will be the uncertain difference in amplitude.

5.2 Halos and Galaxies

Discussion in this paper has assumed, so far, that galaxy clustering and halo clustering are the same thing. Although this is a reasonable assumption if we are interested in only one epoch with an appropriate choice of minimum halo mass, the same is not true for the relative evolution of the two distributions. Here, we list some plausible alternatives and outline the evolution of galaxy correlation function for each one.

At any given epoch, there are more low mass galaxies than high mass galaxies. This suggests that the galaxy correlation function is dominated by the smallest galaxies[¶]. In such a case, the galaxy correlation function must evolve in a manner similar to the halo correlation function and its amplitude must go through a minimum at some epoch. For low mass galaxies, this minimum could be at $z \gg 0$.

The assumption outlined above applies in a much better way to quasars as these cannot form in very low mass halos and the redshift at which the amplitude of quasar correlation reaches the minima may be low enough to be observable. If the minimum halo mass associated with quasars is greater than $10^{11} M_\odot$ then the observed quasar correlation function should have a higher amplitude at $z > 2$ than at $z < 0$. Recent estimates of the quasar correlation function, though based on small datasets, show that clustering of quasars is indeed stronger at higher redshifts (Kundic 1997; La Franca, Andreani and Cristiani 1997). Authors of the second paper claim that the observed evolution of quasar clustering cannot be explained in all models of AGN activity. Our analysis suggests that this need not be true. Quasars must show decreasing clustering amplitude if the AGN activity is not correlated with the large scale environment.

The assumption of a mass threshold also applies very well to groups and clusters of galaxies. Therefore, the cluster correlation function should show a decreasing trend or very slow evolution.

We can use a different ansatz: we can assume that the brightest galaxies reside in halos that have formed relatively recently. We can identify the mass scale $M_*(z)$ by assuming

[§] If we assume the difference between halo clustering and mass clustering to be the only source of error, then we can estimate its magnitude from simulations. The curves for $z = 0$ in fig.3 show this difference to be $\Delta n \simeq 0.2$ for $M_{halo} \geq 2 \times 10^{12} M_\odot$, twice the uncertainty of 0.1 we used in our example.

[¶] There is, of course, the problem of identifying the *same* population of galaxies at different redshifts

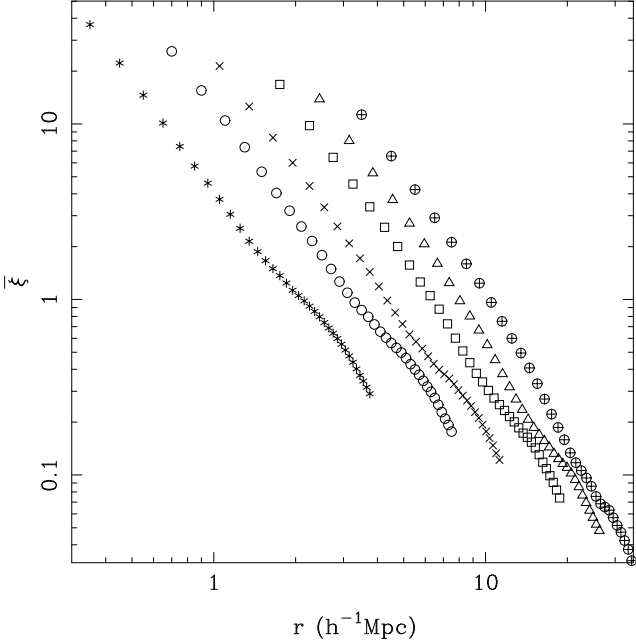


Figure 7. This figure shows evolution of the averaged correlation function of $M_*(z)$ galaxies for the standard CDM model. We have plotted $\bar{\xi}_{halo}$ for halos of different masses at the redshift when $M_{halo} = M_*(z)$. The symbols are: * for $M_{halo} \geq 5.6 \times 10^9 M_\odot$ and $z = 3$, ○ for $M_{halo} \geq 4.5 \times 10^{10} M_\odot$ and $z = 2$, x for $M_{halo} \geq 1.5 \times 10^{11} M_\odot$ and $z = 1.5$, □ for $M_{halo} \geq 7 \times 10^{11} M_\odot$ and $z = 1$, △ for $M_{halo} \geq 2 \times 10^{12} M_\odot$ and $z = 0.5$, and, ⊕ for $M_{halo} \geq 5.6 \times 10^{12} M_\odot$ and $z = 0.25$.

that these correspond to $\nu(M_*) \simeq 1$. Fig.7 shows the halo correlation function for all the simulations listed in table 1 at the epoch when the amplitude of correlation function is minimum. This shows that the correlation function of $M_*(z)$ galaxies is a monotonically growing function of time. The rate of growth for the amplitude of this function is faster than the linear growth rate. This may be a good model for evolution of clustering of faint galaxies (Brainerd, Smail and Mould 1995).

The above discussion shows that the evolution of galaxy clustering is likely to depend strongly on our choice of “galaxies” at different redshifts. If we identify similar objects at different redshifts, then these will show either a decreasing correlation function or nearly constant clustering in comoving co-ordinates. On the other hand, if we are working with the most prominent/numerous objects at each redshift then we should see rapid evolution of clustering. Gastrophysical effects, in general, make the relation of halos and galaxies a little fuzzy, and this will result in an uncertain linear combination of the two types of evolution of clustering.

Considering the uncertain relation of the relative evolution of galaxy/halo and mass clustering, the rate of growth of the correlation function at large scales should not be interpreted as the linear growth rate of density perturbations. Direct determination of cosmological parameters by assuming the two rates to be identical can lead to wrong results.

5.3 Galaxy Clustering and Reionisation of the IGM

Observations show that the Inter-Galactic Medium (IGM) is ionised at the highest redshifts we can probe using known quasars and galaxies. Scenarios for reionisation of the IGM fall in two basic categories: Ionisation by quasars, which have a low number density and hence the IGM has a very patchy structure at early times. Ionisation by proto-galaxies, dwarf galaxies or star clusters that are distributed uniformly, leading to a quick and homogeneous reionisation.

We have shown in this paper that halos, irrespective of their mass, cluster very strongly at early times. Therefore, the reionisation of the IGM will be patchy at a scale much larger than $n^{-1/3}$, where n is the number density of the sources of ionisation. The non-uniformity of halos at early times is illustrated in fig.1.

It is thought that the earliest clusters of stars formed when low mass halos $M_{halo} \simeq 10^6 M_\odot$ collapse after cooling by H_2 line cooling (Tegmark et al. 1997). If these clusters of stars were responsible for reionisation of IGM, then, as these have a very large number density, $n^{-1/3} \approx 10 \text{kpc}_{proper}$, the ionisation structure of the IGM will be fairly homogeneous. However, UV radiation from the first clusters leads to dissociation of H_2 molecules and hence the Jeans mass increases by a considerable amount (Haiman, Rees and Loeb 1997). The second generation of collapsed object are like dwarf galaxies $M_{halo} \simeq 10^{8-9} M_\odot$ and these have a slightly lower number density, $n^{-1/3} \approx 0.1 \text{Mpc}_{proper}$. A visual comparison with fig.1 suggests that some parts of the Universe will be at a much greater distance from the nearest source of ionising radiation. Therefore, one may expect patchiness at scales of 1Mpc_{proper} , or about 10Mpc_{comov} . The early stages of reionisation from such sources may be observed using the 21cm tomography type of observations, though at a scale smaller than that suggested for quasars (Madau, Meiksin and Rees 1997).

The relative distribution of halos and the underlying mass in fig.1 suggests that halos form preferentially along filaments/pancakes or their intersections. Here we present a simple, geometrical model to develop a feel for the manner in which ionisation fronts from such sources evolve before they begin to overlap with one another. Fig.8 shows the Strömgren radii for a point source embedded in a filament. We have assumed that the filament has a radius of 10kpc and is surrounded by an under-dense region. The density in the filament is 5 times the average density (at redshift $z = 10$) and the under-dense region has 0.5 times the average density. We have assumed that $\Omega_b = 0.05$ for the purpose of the following discussion. The Strömgren radii correspond to energy $5 \times 10^{51} \text{ergs}$, $2 \times 10^{52} \text{ergs}$, $8 \times 10^{52} \text{ergs}$, and, $3.2 \times 10^{53} \text{ergs}$ in ionising radiation, assuming that all of the Ly α photons lead to an ionisation. The outermost curve requires energy equivalent of about 10^2 type O stars spread over the time it takes to ionise this region. It is clear from the shape of the contours that the ionisation front does not move as rapidly into the filament as it does into the under-dense region. This has some important implications:

- Under-dense regions get ionised before the filaments and pancakes are completely ionised. If the sources of ionisation are transient, i.e. these switch off after some stage, then under-dense regions will remain ionised as the recom-

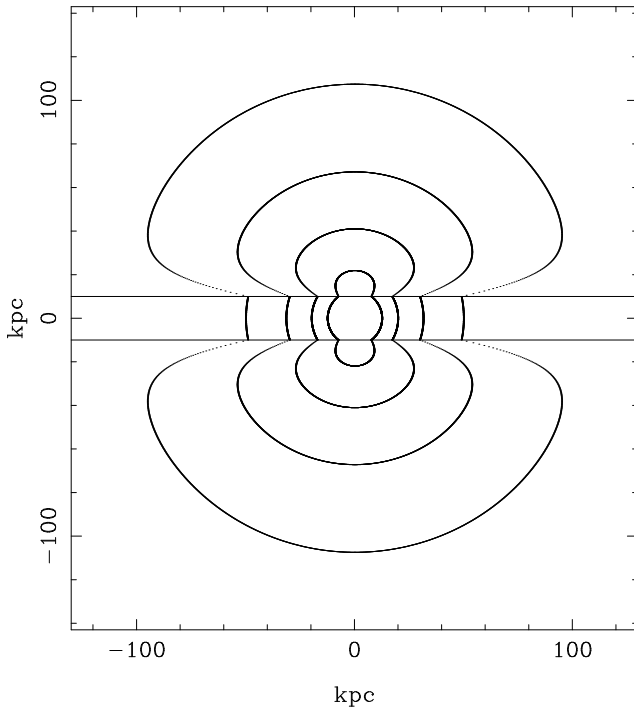


Figure 8. This figure shows the Strömgren radii for a source embedded in an over dense filament surrounded by an under dense region. The Strömgren radius has been plotted for energies 5×10^{51} ergs, 2×10^{52} ergs, 8×10^{52} ergs, and, 3.2×10^{53} ergs in ionising radiation, assuming that all of the Ly α photons lead to an ionisation. The filament has a radius of 10kpc. The density in the filament is 5 times the average density (at redshift $z = 10$) and the surrounding under-dense region has density 0.5 times the average density. We have assumed that $\Omega_b = 0.05$. The outermost contour requires energy equivalent of about 10^2 type O stars spread over the time it takes to ionise this region. It is clear from the shape of the contours that the ionisation front does not move as rapidly into the filament as it does into the under-dense region.

bination time scale for under-dense regions is much longer than the equivalent time scale in over-dense regions.

- Filaments and pancakes are more lumpy than the under-dense regions, therefore it is more probable to have high column density systems along the large scale network. Therefore, the distribution of such systems at high redshifts may be well correlated with the galaxy distribution without (all) such systems being directly associated with galaxies.

- Photo-ionisation in the under-dense region will increase the Jeans mass and suppress collapse of low mass halos (Efstathiou 1992) at late times. This may be the reason for the apparent lack of dwarf galaxies in voids. This effect will not be as prominent in the filaments as the recombination time is smaller, and, ionisation proceeds much more slowly along over-dense regions than it does in the under-dense regions. Also, the typical mass of halos collapsing along the large scale network is higher than the halos collapsing in under-dense regions at the same redshift.

It is clear from the significance of issues relate to this problem that a more detailed analysis of evolution of reionisation is needed. This analysis must account for both radiation transport and the inhomogeneous background mass distribution for it to resolve these questions.

6 CONCLUSIONS

In §5, we have highlighted some implications of the model and simulation results presented in this paper. Our conclusions are summarised below:

- The correlation function of galaxies at high redshifts is considerably higher than the correlation function for the mass distribution. Therefore, large concentrations of galaxies at high redshifts (Steidel et al 1997) are expected in most models of structure formation (Bagla 1997). For example, the halo correlation function of galaxies ($M_{halo} \approx 10^{11} M_\odot$) at $z = 3$ is comparable to the observed galaxy correlation function today.
- The halo correlation function (and the correlation function of mass contained in halos) has a different shape, as compared to the non-linear correlation function of mass. Therefore, inverting the galaxy correlation function to obtain the linear correlation function or the power spectrum can lead to wrong answers at small scales ($l \leq 10 h^{-1} \text{Mpc}$).
- The growth rate of correlation function should not be used, directly, to compute omega/lambda by assuming linear growth or stable clustering.
- Quasar correlation function, as it corresponds to high mass halos, should show a decreasing phase at $z > 1$.
- Cluster correlation function should also show a decreasing phase, if we can define a sample of clusters at higher redshifts ($z \simeq 0.5$) with the same mass threshold.
- The rapid evolution of clustering of faint galaxies can be understood if these correspond to M_* galaxies at high redshifts.
- Earliest structures to form in the Universe will cluster strongly, therefore the sources that reionise the Universe will occur in groups that are further apart than expected from their number density and a nearly uniform distribution. This implies that the reionisation will be very patchy and it may be possible to observe the patchiness using the redshifted 21cm radiation (Madau, Meiksin and Rees 1997).
- Strong clustering of sources of ionising radiation may influence the distribution of QSO absorption systems and dwarf galaxies, as suggested by the simple model presented in §5.3. We are investigating this issue in greater detail.

ACKNOWLEDGEMENT

I would like to thank Martin Rees, K.Subramanian, Ofer Lahav and Shiv Sethi for many useful discussions. I acknowledge the support of PPARC fellowship at the Institute of Astronomy.

REFERENCES

Bagla J.S. and Padmanabhan T. 1997, MNRAS 286, 1023
 Bagla J.S. 1997, Submitted to MNRAS, astro-ph/9707159
 Bardeen J.M., Bond J.R., Kaiser N. and Szalay A.S. 1986, ApJ 304, 15
 Brainerd T.G. and Villumsen J.V. 1994, ApJ 431, 477
 Brainerd T.G., Smail I. and Mould J. 1995, MNRAS 275, 781
 Catelan P., Lucchin F., Matarrese S. and Porciani C. 1997, astro-ph/9708067
 Efstathiou G. 1992, MNRAS 256, 43p
 Fry J.N. 1996, ApJL 461, 65

Gelb J.M. and Bertschinger E. 1994a, *ApJ* 436, 467
 Gelb J.M. and Bertschinger E. 1994b, *ApJ* 436, 491
 Gunn J.E. and Gott J.R. 1972, *ApJ* 176, 1
 Haiman Z., Rees M.J. and Loeb A. 1997, *ApJ* 476, 458
 Hamilton A.J.S., Kumar P., Edward Lu and Matthews A. 1991,
 ApJL 374, 1-4
 Kundic T. 1997, *ApJ* 482, 631
 La Franca F., Andreani P. and Cristiani S. 1997, astro-
 ph/9711048, to appear in *ApJ*
 Madau P., Meiksin A. and Rees M.J. 1997, *ApJ* 475, 429
 Matarrese S., Coles P., Lucchin F. and Moscardini L. 1997, *MNRAS* 286, 115
 Mo H.J. and White S.D.M. 1996, *MNRAS* 282, 1096
 Moore B., Katz N. and Lake G. 1996, *ApJ* 457, 455
 Ogawa T., Roukema B.F. and Yamashita K. 1997, *ApJ* 484, 53
 Peacock J.A. and Dodds S.J. 1996, *MNRAS* 280, 19
 Steidel C.C., Adelberger K.L., Dickinson M., Giavalisco M., Pet-
 tini M. and Kellogg M. 1997, *ApJL*, In Press
 Tegmark M., Silk J., Rees M.J., Blanchard A., Abel T. and Palla
 F. 1997, *ApJ* 474, 1

This figure "fig1a.gif" is available in "gif" format from:

<http://arxiv.org/ps/astro-ph/9711081v1>

This figure "fig1b.gif" is available in "gif" format from:

<http://arxiv.org/ps/astro-ph/9711081v1>

This figure "fig1c.gif" is available in "gif" format from:

<http://arxiv.org/ps/astro-ph/9711081v1>

This figure "fig1d.gif" is available in "gif" format from:

<http://arxiv.org/ps/astro-ph/9711081v1>